



# Oil palm waste-derived adsorbents for the sequestration of selected polycyclic aromatic hydrocarbon in contaminated aqueous medium

God'swill Nathan Sambo<sup>1</sup> · Adedapo Oluwasanu Adeola<sup>2</sup> · Syahidah Akmal Muhammad<sup>1,3</sup>

Received: 6 March 2023 / Accepted: 24 March 2024  
© The Author(s) 2024

## Abstract

Carbonaceous adsorbents were synthesized from palm kernel shell and palm mesocarp fiber for the adsorption of phenanthrene (PHE) and the highly carcinogenic-benzo(a)pyrene (BaP). The structure and properties of the activated biochar were characterized using standardized analytical tools. The microscopic examinations carried out with SEM and BET results revealed mesoporous structures and interstitial spaces in the activated samples (AB-PKS and AB-PMS). Powder X-ray diffraction (PXRD) results showed that prepared sorbents are amorphous and that activation affected the amorphous cellulose on the surface of the microfibrils which led to a decrease in the intensity of some peaks. Fourier-transform infrared spectroscopy (FTIR) affirms the availability of surface moieties that may promote polycyclic aromatic hydrocarbon (PAH) removal or decontamination of aqueous media. The sorption isotherm and effect of pH on the adsorption of PHE and BaP onto the activated palm kernel shell (AB-PKS) and activated palm mesocarp fiber (AB-PMF) were investigated. The isotherm studies and error analysis (SSE and  $R^2$ ) confirm that the Freundlich model best fits experimental results for AB-PMF; while, the Langmuir model best describes AB-PKS sorption of BaP and PHE, respectively. The optimal removal efficiency for PHE was between 84 and 100% while that of BaP was between 68 and 87% with maximum adsorption capacity ( $q_{max}$ ) of 19.38–21.98 mg/g and 1.24–13.26 mg/g, respectively. The optimum pH condition for removing PHE is less than 7 and above 7 for BaP. Therefore, the conversion of waste materials to useful sorbents, as well as preliminary adsorption test results obtained suggests a cleaner and cost-effective pathway for waste management and water treatment.

**Keywords** Benzo(a)pyrene · Biochar · Palm kernel shell · Palm mesocarp fiber · Phenanthrene · Water treatment

## Abbreviations

AB-PKS Palm kernel shell-activated biochar  
AB-PMF Palm mesocarp fiber-activated biochar  
BaP Benzo(a)pyrene

B-PKS Palm kernel shell biochar  
B-PMF Palm mesocarp fiber biochar  
BET Brunauer–Emmett–Teller  
CO<sub>2</sub> Carbon dioxide  
FM Freundlich model  
FTIR Fourier-transform infrared spectroscopy  
GC-FID Gas chromatography with flame ionization detection  
H<sub>2</sub>O Water  
HCl Hydrochloric acid  
H<sub>3</sub>PO<sub>4</sub> Phosphoric acid  
HNO<sub>3</sub> Nitric acid  
KOH Potassium hydroxide  
LM Langmuir model  
NaOH Sodium hydroxide  
PAHs Polycyclic aromatic hydrocarbons  
PHE Phenanthrene  
PKS Palm kernel shell  
PMF Palm mesocarp fiber  
SDGs Sustainable development goals

✉ God'swill Nathan Sambo  
geogodswills@gmail.com

✉ Adedapo Oluwasanu Adeola  
adedapo.adeola@aau.edu.ng

✉ Syahidah Akmal Muhammad  
syahidah.muhammad@usm.my

<sup>1</sup> Environmental Technology Division, School of Industrial Technology, Universiti Sains Malaysia, 11800 USM, Penang, Malaysia

<sup>2</sup> Department of Chemical Sciences, Adekunle Ajasin University, PMB 001, Akungba-Akoko, Ondo State, Nigeria

<sup>3</sup> Analytical Biochemistry Research Centre (ABrC), Inkubator Inovasi Universiti (I2U), Kampus SAINS@USM, Universiti Sains Malaysia, Lebuh Bukit Jambul, 11900 Bayan Lepas, Penang, Malaysia

SEM	Scanning electron microscope
TEM	Transmission electron microscopy
WHO	World Health Organization
XRD	X-ray diffraction
ZnCl <sub>2</sub>	Zinc chloride

## Introduction

Water pollution is a growing global challenge that has detrimental implications for both human health and the environment. Furthermore, water is not readily available in certain parts of the world as about 4 billion people are faced with water shortage for a minimum of one month each year based on the United Nations World Water Development Report in 2020 (Pltonykova et al. 2020). Based on projections, water scarcity will increase to about 9.4–10.2 billion in 2050 as a result of the growing global population (Boretti and Rosa 2019). Owing to this, access to safe water for everyone regardless of their economic situation or social standing is one of the main objectives of the World Health Organization (WHO). Additionally, the Sustainable Development Goals (SDGs) seek to address problems with water, such as water pollution, flooding, and drought (Adeola and Forbes 2021). It is, therefore, imperative to continuously design sustainable ways of treating and recycling polluted water and/or wastewater.

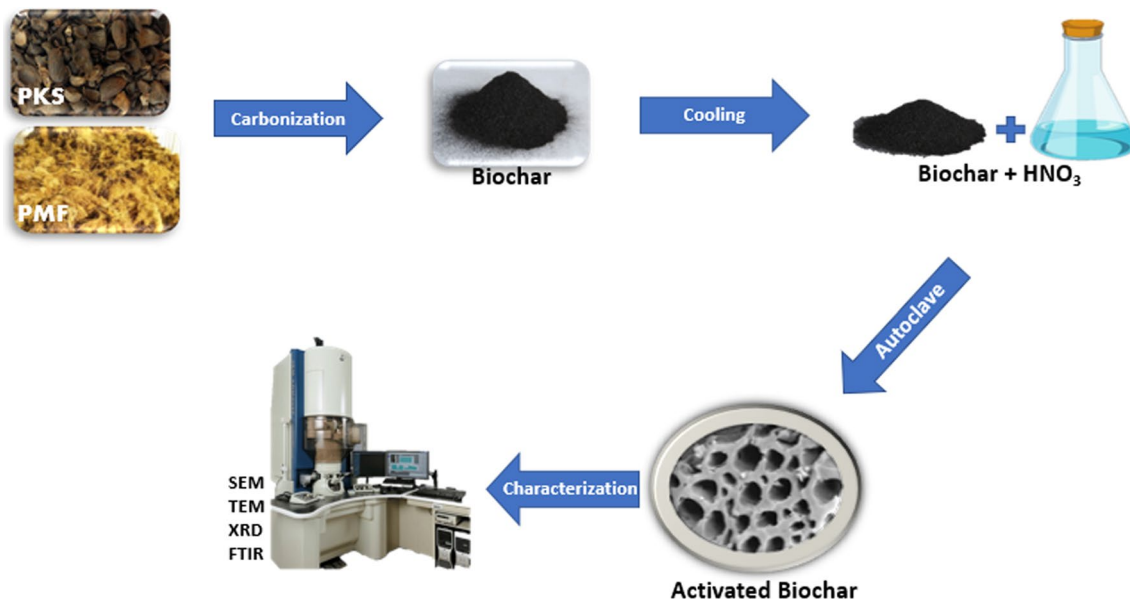
Sewage, agricultural, and industrial waste, including chemicals, grease, oil, and other harmful materials are the leading sources of water pollutants (Priyadarshini et al. 2022). In recent times, there has been a notable increase in the number of chemical products available to the global market. Pharmaceuticals, polycyclic aromatic hydrocarbons (PAHs), surfactants, and pesticides are among the bulk of them. These substances are used in industrial and agricultural processes and are eventually discharged into water bodies, posing substantial environmental and health risks. According to research, organic contaminants such as PAHs can be found in a variety of aquatic settings (Sambo et al. 2022). Though numerous harmful chemicals are potentially generated at such locations, PAHs are a pervasive group of organic pollutants generated by human activities through industrialization and urbanization (Kubheka et al. 2022).

PAHs like phenanthrene (PHE) and benzo(a)pyrene (BaP) are organic pollutants that are hydrophobic, slightly volatile, and environmentally ubiquitous. It can mostly be found as mixtures in sediments, soil, air, water, and biota, which is mostly caused by subsurface fuel pipeline leaks, effluent discharge from the petroleum and petrochemical sectors, and gasoline leaks from storage tanks (Jesus et al. 2022). Through ingestion, inhalation, and skin contact, PAHs can permeate the human body and eventually build up in epithelial tissue, the liver, and the blood, thus posing severe

health challenges (Dehghani et al. 2022). The United States Environmental Protection Agency has designated 16 PAHs (including PHE and BaP) as priority pollutants because they have carcinogenic or mutagenic properties and are very persistent in the environment. It is therefore important for PAHs to be treated in environmental media.

According to Hoang et al. (2022), the adsorption technique has demonstrated greater performance in water and wastewater treatments compared to other technologies in terms of process cost, flexibility, user-friendly design, ease of operation, and high sensitivity threshold to harmful pollutants. Also, the use of the adsorption technology is advantageous because no harmful compounds are created during the process of treatment. Due to the availability of agricultural waste, the utilization of biomass and agricultural waste as adsorbent stands out as it has proven to be suitable, simple, and cost-effective. It provides a useful method for managing waste because it enables the transformation of “waste to wealth” (Sambo et al. 2022). Research has reported the adsorption of PAHs in water using agricultural wastes like rice husk (Guo et al. 2018), wood waste-derived biochar (Zhou et al. 2022), sunflower husk (Minkina et al. 2022), and corn straw biochar (Guo et al. 2020). Biomass is usually converted to either biochar or activated carbon before its application in adsorption processes. When biochar is activated, either using gaseous agents like H<sub>2</sub>O or CO<sub>2</sub>, or chemical agents like KOH, H<sub>3</sub>PO<sub>4</sub>, or ZnCl<sub>2</sub>, the surface area will be significantly increased, enhancing its ability to adsorb pollutants. However, the activation procedure frequently requires high-temperature processing, chemicals with high concentrations, and specialized equipment, all of which raise energy consumption, waste, and capital costs, respectively (Ibrahim et al. 2021). It is therefore essential to research a strategy to enhance biochar’s surface characteristics using current technology that uses less energy and produces less secondary waste. Palm oil is a global commodity, and with high demand comes the burden of large production and its associated solid wastes. We thus want to gain valuable insight into sorbents generated from the fibrous parts of the plant and waste generated from its fruits (palm kernel shells). The chemistry of carbon materials is often influenced by the nature of their precursors. Furthermore, we chose two 3-ringed PAH (phenanthrene) and 5-ringed PAH (benzo(a)pyrene) to investigate the role of difference in the molecular weight and structure may have on the adsorption capacity of the synthesized biomass-based sorbent.

This work aims to determine the adsorption of PHE and BaP in water by palm kernel shell and palm mesocarp fiber that is activated using nitric acid in an autoclave. Therefore, this study was conducted using a low concentration of HNO<sub>3</sub>, and a quick and facile procedure compared to other surface functionalization procedures that were previously reported. The nitric acid was used to improve the



**Scheme 1** Schematic representation of preparation process of biochar and activated biochar from palm kernel shell and palm mesocarp fiber

characteristics of the biochar; while, an autoclave was employed to improve and speed up the activation process. The role of pH, dosage, and initial concentration of PHE and BaP on the adsorption capacity of the two adsorbents (namely palm kernel shell-activated biochar (AB-PKS) and palm mesocarp fiber-activated biochar (AB-PMF)) were investigated to determine the optimal conditions for effective water purification.

## Materials and method

### Preparation of adsorbents

The batch study of the adsorption of PHE and BaP was conducted using AB-PKS and AB-PMF. Raw palm kernel shell and palm mesocarp fiber were collected from United Oil Palm Industries Sdn. Bhd, Penang, Malaysia. The samples were washed multiple times using distilled water to remove dirt and surface impurities. The washed samples were then oven-dried at 105 °C for 24 h after which they were allowed to cool at room temperature. The samples were separately pulverized and sieved through a 2 mm membrane. To create palm kernel shell biochar (B-PKS) and palm mesocarp fiber biochar (B-PMF), 50 g of each sample were pyrolyzed in a furnace at a rate of 15 °C/min until it reached 450 °C then it was left in the furnace for 30 min. The samples were then rinsed with 0.1 M HCl and ultra-pure water until a pH of 6–7 was achieved, after which it was oven-dried at 75 °C for 24 h. To functionalize the biochar surface, 5 g of B-PKS and B-PMF were separately weighed into an Erlenmeyer flask, and 100 mL

of 1 M of HNO<sub>3</sub> was added to the flask and carefully covered with foil paper to avoid spillover. The set-up was placed in an autoclave at 121 °C at 100 kPa for 2 h. It was then allowed to cool to 60 °C, and the treated biochar was washed with distilled water and 0.01 M NaOH until a pH of 6–7 was achieved. The adsorbents (AB-PKS and AB-PMF) were then oven-dried for 24 h at 75 °C and kept in a desiccator for characterization. The biochar yield was calculated using the following:

$$\text{Biochar yield (\%)} = \frac{\text{weight of dry biochar}}{\text{weight of biomass}} \times 100 \quad (1)$$

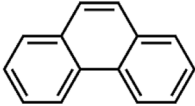
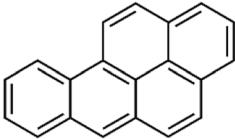
### Characterization of adsorbents

The surface morphology of B-PKS, B-PMF, AB-PKS, and AB-PMF were obtained from the scanning electron microscopy (Zeiss Ultra-Plus 55 field emission SEM, ZEISS, Germany); while, the inner structures of the samples were determined using the transmission electron microscope (ZEISS, Germany). The functional groups present in the samples were determined from Fourier-transform infrared spectroscopy (FTIR) (Bruker Optik GmbH, Ettlingen, Germany). Powdered X-ray diffraction (PXRD) patterns were obtained using the Bruker D8 Advance, Karlsruhe, Germany (Scheme 1).

### Adsorption isotherm experiment

PHE standard ( $\geq 97\%$  purity) and BaP standard ( $\geq 98\%$  purity) were purchased from Shanghai Macklin Biochemical Co., Ltd. Stock solution (100 mg/L) of PHE and BaP

**Table 1** Basic properties of the selected polycyclic aromatic hydrocarbons (PAH)

PAH	Molecular Structure	Molecular formula	LogK <sub>ow</sub>	S <sub>w</sub>	M <sub>w</sub>	B <sub>p</sub>
Phenanthrene		C <sub>14</sub> H <sub>10</sub>	4.57	1.6	178.23	332
Benzo(a)pyrene		C <sub>20</sub> H <sub>12</sub>	5.91	0.0038	252.32	495

Log K<sub>ow</sub>: octanol–water partition coefficient, S<sub>w</sub>: water solubility (mg/L), M<sub>w</sub>: molecular weight (g/mol), B<sub>p</sub>: boiling points (°C). Cited from PubChem

was prepared in water–methanol solution (80:20%) to facilitate complete dissolution of PAHs. The batch adsorption of PHE and BaP was conducted in 20 mL of water for 48 h at 150 rpm at a temperature of 25 ± 1 °C in amber containers covered with foil paper. The isothermal studies were done with initial PHE and BaP concentrations ranging from 5 to 35 mg/L and an adsorbent dose of 20 mg. The pH effect on the adsorption was conducted using a pH in the range of 3–11. The pH was adjusted using 0.1 M NaOH or HCl.

## Quantification

The PHE and BaP concentrations were analyzed with the aid of gas chromatography with a flame ionization detector (GC-FID). The helium carrier gas at a constant flow mode, 32 cm/s at 40 °C. The column used was an Agilent J&W DB-5 ms Ultra Inert, (30 m × 0.25 mm, 0.25 μm). The oven temperature was programmed at 40 °C (1 min); 30 °C/min to 160 °C; 6 °C/min to 300 °C (5 min). The regression coefficients (*R*<sup>2</sup>) of matrix-matched calibration curves were established from the PHE and BaP concentration range of 5–30 mg/L. The equilibrium concentration (*C*<sub>e</sub>) and solute adsorbed (*q*<sub>e</sub>) were determined using the equation below:

$$q_e = \frac{(C_0 - C_e)V}{m} \quad (2)$$

where *C*<sub>0</sub> is the initial concentration (mg/L), *C*<sub>e</sub> is the equilibrium solute concentration, *m* is the mass (mg) and *V* is the initial volume of PAH solution (mL). Table 1 presents the properties and structures of the target pollutants used in this study.

**Table 2** Yield of biochar after carbonization

Sample	Mass of biomass (g)	Biochar yield (g)	Biochar yield (%)	pH
B-PKS	50	16.29	32.58	7.68
B-PMF	50	11.32	22.65	8.1

**Table 3** Yield after activation

Sample	Mass of bio-char (g)	Activated biochar yield (g)	Activated biochar yield (%)
AB-PKS	5	4.72	94.4
AB-PMF	5	4.93	98.6

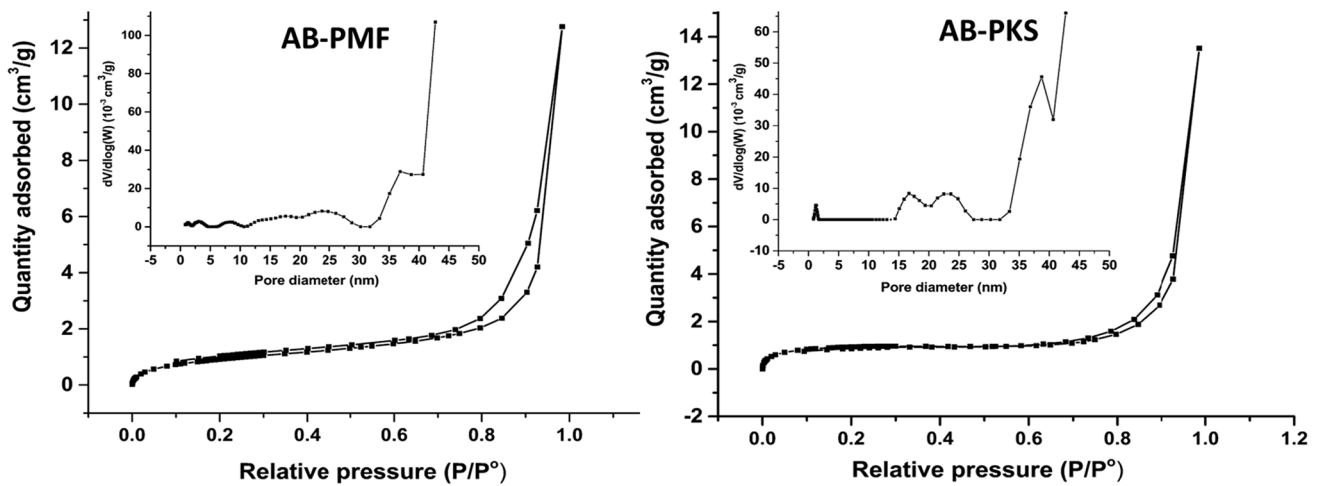
## Results and discussions

### Yield of carbonization and activation

The yield of the B-PKS and B-PMF was 32.58% and 22.65%, respectively, after carbonization as shown in Table 2. This result is similar to the report of previous works with a range of 20–45% (Claoston et al. 2014; Idris et al. 2015). After activation of 5 g of B-PKS and B-PMF, the activated biochar produced was about 94–99% as shown in Table 3. This loss in yield can be attributed to the process of sample rinsing and transfer. It, therefore, indicates that the activation process does not influence the bulk structure of the biochar, but only influences the surface of the biochar (Ibrahim et al. 2021).

### BET analysis

AB-PMS and AB-PKS's pore size distribution plot and Brunauer–Emmett–Teller (BET) isotherm are shown in



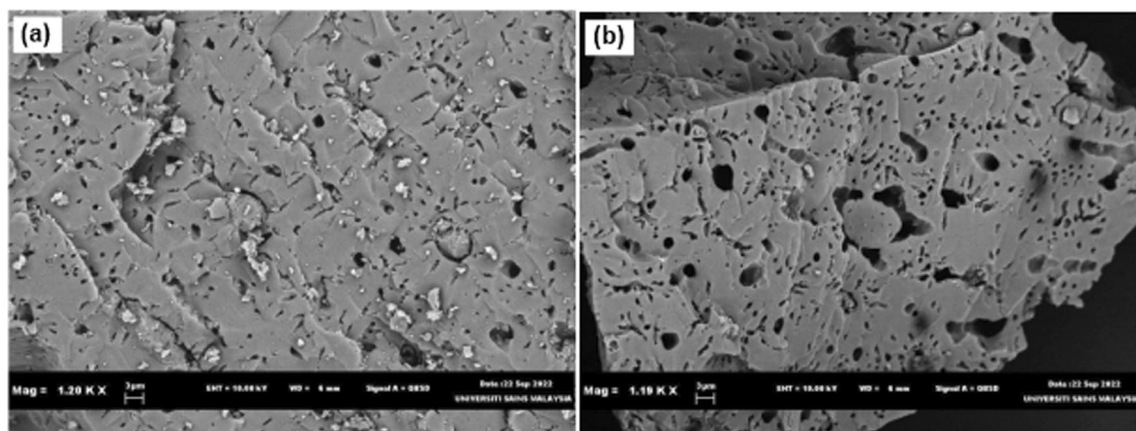
**Fig. 1** N<sub>2</sub> sorption isotherm curves of activated biochar (AB-PKS) and activated biochar (AB-PMF) with insets showing the pore size distribution

Fig. 1. The N<sub>2</sub> isotherm plots show a type IV isotherm that is frequently connected to mesoporous materials; taking into account the hysteresis loops with small variation in the sorption reversibility of the AB-PKS and AB-PMF (Bowker 2012). The pore distribution showed that both sorbents are primarily mesoporous (between 2 and 50 nm), with a BJH average pore diameter ranging between 35 and 40 nm, despite the presence of micropores (with sizes less than 2 nm) (Pavlenko et al. 2022). According to the estimates, the specific surface area (SSA) was 211.02 m<sup>2</sup>/g (AB-PMF) and 134.70 m<sup>2</sup>/g (AB-PKS).

**SEM analysis**

The SEM images of B-PKS, B-PMF, AB-PKS, and AB-PMF are shown in Figs. 2, 3. The images revealed a smooth, compact, and non-fibrous structure which is due

to the presence of hemicellulose and lignin in the samples (Nascimento et al. 2016). Considering Figs. 2a, 3a, acid treatment may have removed some particulate matter from the surface of the untreated biochar as shown in Figs. 2b, 3b. This particulate matter may include silica and other minerals as previously reported by Nguyen (2021). This was equally indicated by the development of mesopores which were previously occupied by silica thereby reducing the adsorption capacity. Natsir et al. (2021) confirmed that silica must be eliminated during the pre-treatment phase to facilitate hemicellulose penetration. In addition, the morphology of the activated biochar became more arranged, reflecting a honeycomb-like pattern with cylindrical holes interconnected by some large holes. According to Feng et al. (2021), biochar with its pore structures organized properly has better adsorptive capacity and a high BET surface area.



**Fig. 2** SEM images of (a) Biochar derived from palm kernel shell (B-PKS) and (b) activated biochar derived from palm kernel shell (AB-PKS)



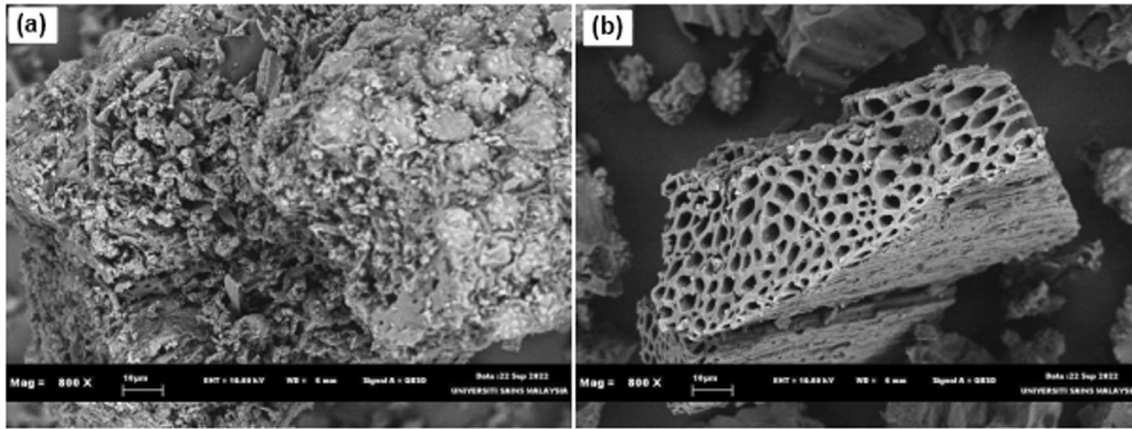


**Fig. 3** SEM images of (a) biochar derived from palm mesocarp fiber (B-PMF) and (b) activated biochar derived from palm mesocarp fiber (AB-PMF)

### XRD analysis

X-ray diffraction (XRD) analysis of B-PKS, B-PMF, AB-PKS, and AB-PMF (Fig. 4) was performed to ascertain the change in crystallinity as a result of the activation process. The graphs show a similar dominant amorphous structure with crystalline peaks that reflect higher cellulose content (Ibrahim et al. 2018; Wan Isahak et al. 2013). From Fig. 4a, the intensity of the graphitic peak at  $29.1^\circ$  significantly decreased after activation. This scenario also played out in Fig. 4b for peaks at  $26.9^\circ$ ,  $29.4^\circ$  and  $43.2^\circ$ . The activation by  $\text{HNO}_3$  affected the amorphous cellulose on the surface of the microfibrils thereby leading to a decrease in the intensity of the peaks (Nurhafizah et al. 2020). However, the intensity

of the broad amorphous peak at  $22.9^\circ$  (Fig. 6a) and  $23.4^\circ$  (Fig. 4b) increased due to the increase in the amorphous lignin that formed during activation (Saleh and Abdul Samad 2022).

### FTIR analysis

Figures 5a and b shows the FTIR spectra peaks for B-PKS, B-PMF, AB-PKS, and AB-PMF. Notwithstanding the general resemblance in the spectra, certain distinctions can be noticed after the activation process. In Fig. 5a, the O–H stretch was observed at  $3396.64\text{ cm}^{-1}$  and this can be attributed to the presence of cellulose and hemicellulose. Two peaks at  $2918.30\text{ cm}^{-1}$  and  $2862.36\text{ cm}^{-1}$  for B-PKS and

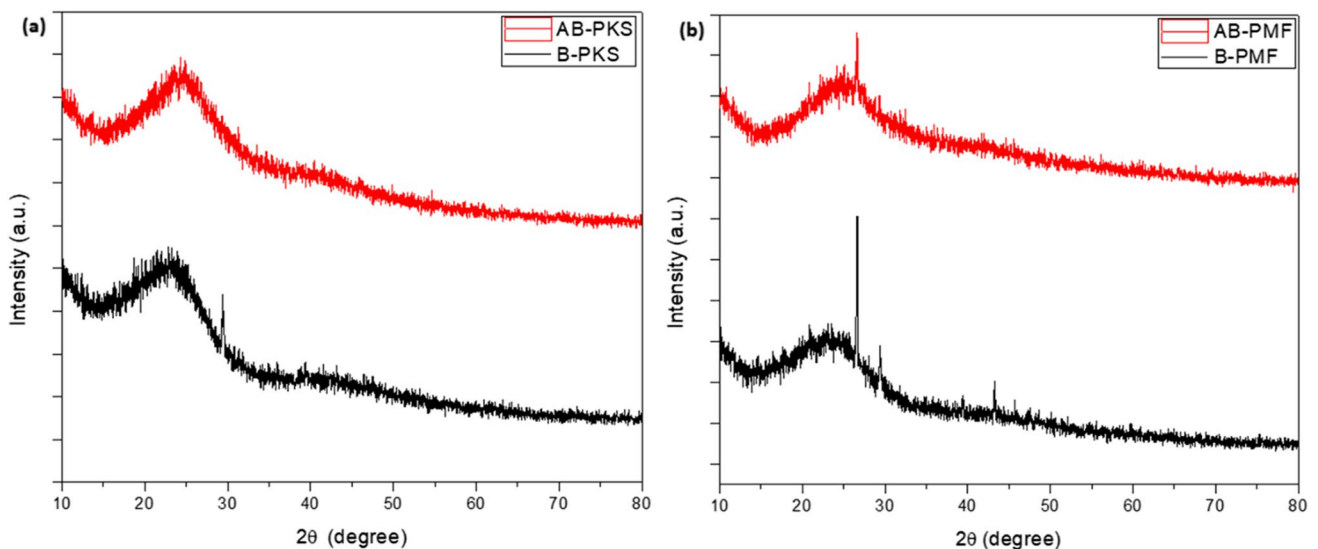


**Fig. 4** XRD patterns for (a) Biochar (B-PKS) and activated biochar (AB-PKS) derived from Palm kernel shell and (b) biochar (B-PMF) and activated biochar (AB-PMF) derived from Palm mesocarp fiber

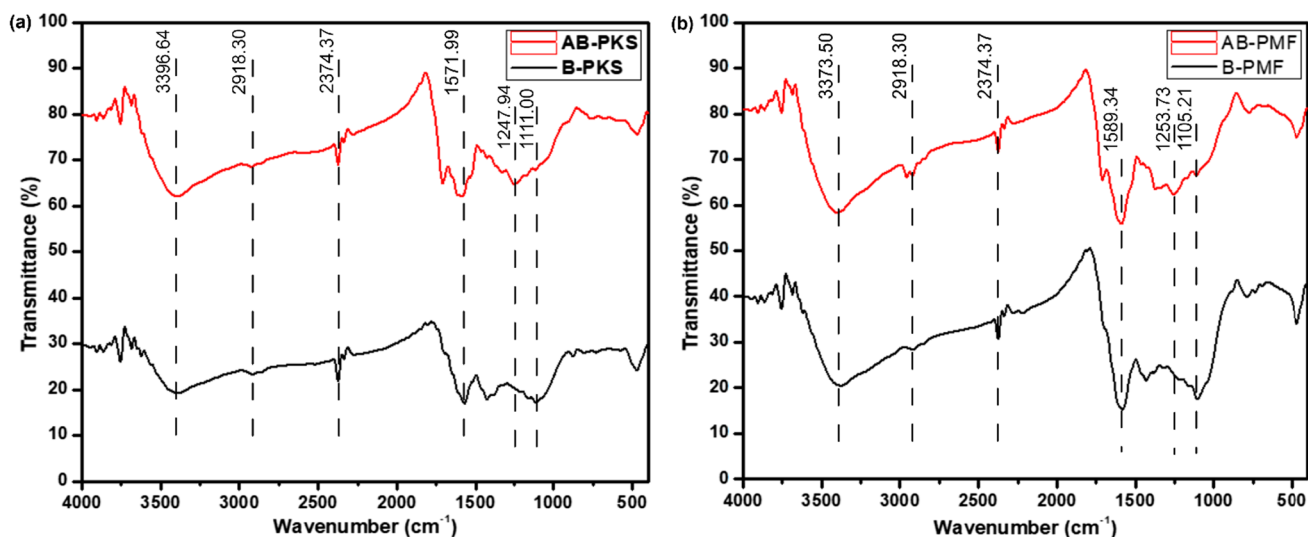


Fig. 5 FTIR spectra peaks for (a) biochar (B-PKS) and activated biochar (AB-PKS) derived from palm kernel shell and (b) biochar (B-PMF) and activated biochar (AB-PMF) derived from palm mesocarp fiber

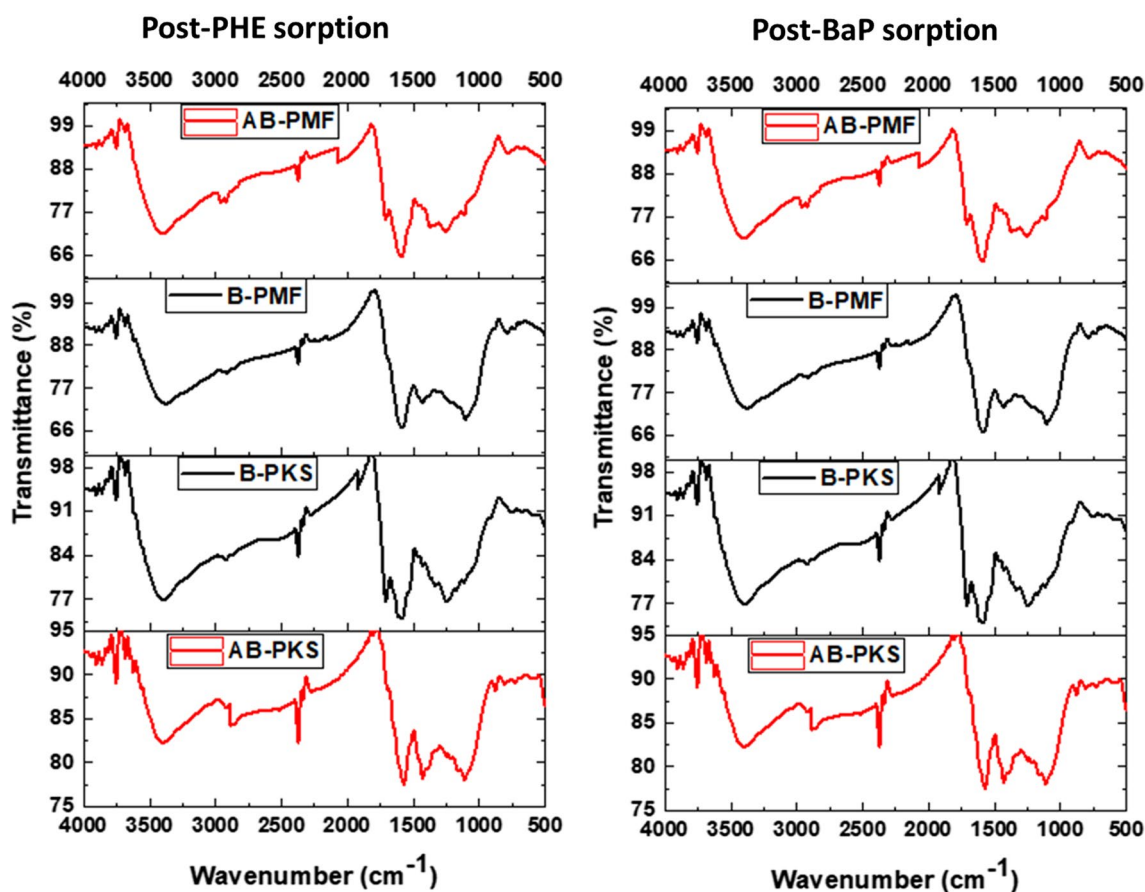


Fig. 6 Post-adsorption FTIR spectra for biochar (B-PKS), activated biochar (AB-PKS) derived from palm kernel shell; and biochar (B-PMF) and activated biochar (AB-PMF) derived from palm mesocarp fiber

around  $2924.09\text{ cm}^{-1}$  for AB-PKS are the C–H vibrational stretch of the aliphatic group. This peak was reduced in AB-PKS after the acid treatment and this favors the removal of PAH (Roy et al. 2021). Bands that are associated with carboxylic groups (C=O) (e.g., ketones, esters, carboxyl) are seen in B-PKS at  $1694.43\text{--}1847.81\text{ cm}^{-1}$  but are not seen in the spectra of AB-PKS (Jouiad et al. 2015). The band associated with aromatic C=C stretching at  $1571.99\text{ cm}^{-1}$  was also reduced in AB-PKS which indicates the removal of lignin (Ibrahim et al. 2018). Finally, at  $1111\text{ cm}^{-1}$ , the band can be assigned to C–O stretch from organic alcohols or esters. Figure 5b also displays a similar scenario for B-PMF and AB-PMF. The broad and strong peaks at  $3373.50\text{ cm}^{-1}$  correspond to the O–H stretching. The C–H vibrational stretch of the aliphatic group was at  $2918.30\text{ cm}^{-1}$  and  $2920.23\text{ cm}^{-1}$  for B-PKS and AB-PKS, respectively. Finally, the C–O stretch from organic alcohols or esters appeared at  $1105.21\text{ cm}^{-1}$ . This peak was greatly reduced after the acid treatment in AB-PMF.

It was also observed that sorbent–sorbate interaction caused peak alteration of some functional groups (peak shape and enhanced intensities) and peak shift in the spectral after PHE and BaP uptake as demonstrated in Fig. 6, respectively. PHE and BaP are aromatic hydrocarbons, composed mainly of C–H, C=C, and C–C bonds, also present in the biomass-derived carbonaceous adsorbents used in this study; hence, the justification for the non-appearance of new peaks, but enhancements and alteration of peak shapes and intensities due to changes in vibrational interactions on the surface of the materials after adsorption. Although the key functional groups captured in Fig. 5 remain present. Peak shifts and enhancements have also been reported by other studies as post-adsorption effects (Pathak et al. 2020; Saleh et al. 2021).

## Adsorption isotherm

At sorption equilibrium, sorbent–sorbate interactions can be better understood using adsorption isotherm models (Zhang et al. 2014). The sorption isotherms of PHE and BaP on AB-PKS and AB-PMF are shown in Fig. 7. The models discussed below were used to fit the adsorption experimental results. These models included the Freundlich, Langmuir, and Linear isotherm models. The Freundlich model (FM), is often used to describe the sorption equilibria of hydrophobic organic compounds, such as PAHs (Eq. 3). The Langmuir model (LM) explains the site-limiting sorption equilibrium (Eq. 4), and the linear equation (Eq. 5) can also be used to explain the partitioning behavior of the chosen PAHs between the sorbent–solution interphase. We used the Sum of Squared Errors (SSE) (Eq. 6) to verify every sorption model.

$$q_e = K_f C_e^N \quad (3)$$

$$q_e = \frac{q_{\max} K_L C_e}{1 + K_L C_e} \quad (4)$$

$$q_e = K_d C_e \quad (5)$$

$$\sum_{i=1}^n (q_{e,\text{cal}} - q_{e,\text{exp}})_i^2 \quad (6)$$

where  $q_e$  is the solid-phase concentration (mg/g), and  $C_e$  is the liquid-phase equilibrium concentration (mg/L).  $K_f$  is the sorption capacity-related parameter,  $K_L$  is the Langmuir constant,  $K_d$  is the partition coefficient/adsorption capacity,

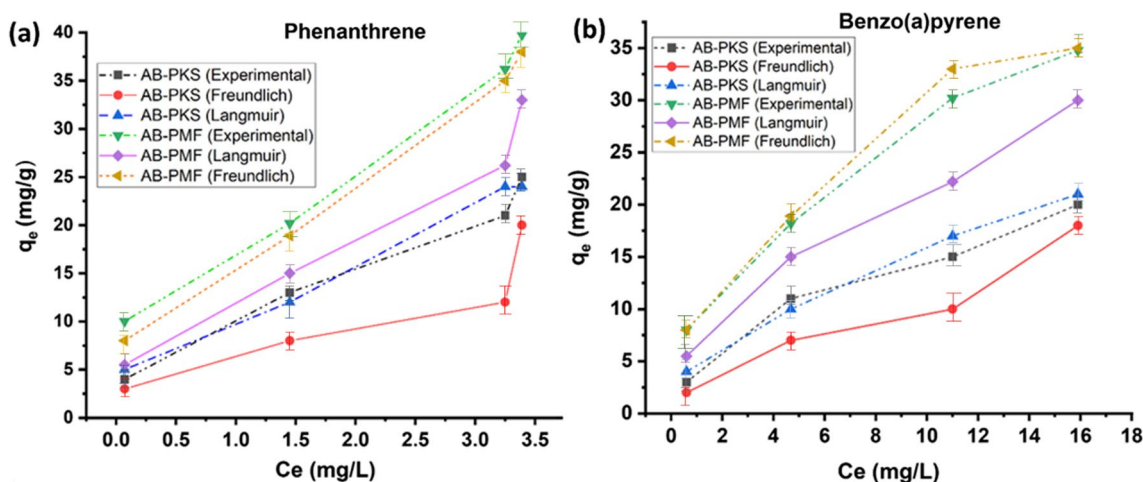


**Fig. 7** Plots of nonlinear fit of isotherm models for PHE and BaP onto AB-PKS and AB-PMF (Best-fit models appear in dotted lines). Error bars  $\pm$  relative standard deviation (RSD),  $n=3$



$N$  is the isotherm nonlinearity index, and  $q_{max}$  is the maximal sorption capacity (Zou et al. 2021).

Table 4 and Fig. 7 show the parameters and isotherm regression graphs for the Freundlich, Langmuir, and linear models. The Freundlich isotherm model best fits the data for BaP and PHE adsorption by AB-PMF sorbents based on the SSE and  $R^2$  values obtained from linear and nonlinear regression and error analysis. On the contrary, The Langmuir isotherm model best fits the data for BaP and PHE sorption onto AB-PKS sorbents based on the SSE and  $R^2$  values obtained. This suggests that while the monolayer adsorption mechanism dominated the adsorption pattern of AB-PKS, the multilayer mechanism prevailed in the sorption process of AB-PMS (Nnaji et al. 2021). The heterogeneous adsorption pattern observed further stresses how variation in sorbent physicochemical properties may influence different compounds' adsorption mechanisms, even if they belong to the same class of chemicals (like in the case of the PAHs used in this study).

The role of electron transfer  $\pi - \pi$  interactions cannot be ruled out as in the case of most carbonaceous adsorbents used for PAH sorption (Wang et al. 2014; Adeola and Forbes 2021). The creation of new adsorption sites results in an increase in the adsorption capacity; hence, the Freundlich constant “ $N$ ” captures the heterogeneity index of the adsorbent's surface and the intensity of the adsorption thereof. This suggests why the maximum adsorption capacity ( $q_{max}$ ) is lower for activated biochar from palm kernel shell (AB-PKS) when compared with values obtained for palm mesocarp fiber (AB-PMF) (Table 4). The higher adsorption capacity of AB-PMF can also be attributed to its tendency to adsorb PAHs in multiple layers (Freundlich), as well as its higher surface area and availability of interstitial spaces (Figs. 1, 2, 3), which could enhance the entrapment of the

respective PAHs (Zhang et al. 2014). Overall, the adsorption capacities for PHE ( $K_d$ ,  $K_F$ , and  $q_{max}$ ) are higher than what was obtained for BaP, which could be attributed to the physicochemical properties of compounds and sorbents (i.e., the lower molecular size of PHE which may facilitate sorbent pore-filling mechanisms) (Akpomie et al. 2022; Zhang et al. 2014).

The selection of an adsorbent for use in water treatment applications depends on several variables, including effectiveness, non-toxicity, material accessibility, flexibility, etc. Table 5 reveals that the adsorbents derived from two different palm wastes are comparatively effective and suitable for the removal of hydrophobic organic pollutants, such as PAHs, from contaminated water. Acidic treatment of biomass increases the acidic characteristic of activated carbon, eliminates mineral components, and enhances the hydrophilic nature of the carbon surface. The Brunauer–Emmett–Teller (BET) surface area of the activated carbon will also be improved after treatment with  $HNO_3$  as research has shown an increase of over 4.93% (Tan et al. 2017). AB-PMF and AB-PKS are very porous and have a very high volume-to-mass ratio (low density). These characteristics make them suitable materials that can be used as packing materials and polishing tools in water treatment applications.

### Effect of pH and sorbent dosage

pH can alter the net charge of the adsorbent and adsorbate; hence, it is crucial for the adsorption of hydrophobic organic molecules (Elwakeel et al. 2017; Kubheka et al. 2022). Since the pH of aqueous environmental systems is not static and varies depending on the nature and composition of the aquatic system, the effect of pH was determined between pH of 3–11 for the adsorption of PHE and

**Table 4** Coefficients obtained from three different sorption isotherm models for PHE and BaP by the biomass-derived adsorbent and their correlation coefficients ( $R^2$ ) and sum of squared error (SSE) (experimental conditions: initial concentration: 5–35 mg/L; dosage: 20 mg per 20 mL; T:  $25 \pm 1$  °C; agitation rate: 150 rpm; contact time: 48 h; pH:  $6.8 \pm 0.2$  for PHE and  $6.5 \pm 0.2$  for BaP)

Isotherm model	Parameter	PAH			
		Phenanthrene		Benzo(a)pyrene	
		AB-PMF	AB-PKS	AB-PMF	AB-PKS
Linear	$K_d$	6.8253	5.2347	0.2211	0.2158
	$R^2$	0.8985	0.7291	0.7314	0.9412
	SSE	0.0788	0.4983	0.9021	1.1650
Freundlich	$N$	2.36	1.35	3.43	2.88
	$K_F$	3.19	2.68	2.12	1.69
	$R^2$	<b>0.9732</b>	0.5424	<b>0.9478</b>	0.8087
	SSE	<b>0.0554</b>	0.0978	<b>0.6450</b>	0.0437
Langmuir	$q_{max}$ (mg g <sup>-1</sup> )	21.98	19.38	13.26	1.24
	$K_L$	4.10	0.86	0.78	0.14
	$R^2$	0.9603	<b>0.9493</b>	0.9327	<b>0.9812</b>
	SSE	0.0565	<b>0.0890</b>	1.1648	<b>0.0389</b>

The bold is for emphasis on the most important data of interest. Captures the best fit model following the values following the correlation coefficient and error squared values

**Table 5** Comparison of different biomass-based materials and their adsorption capacity of phenanthrene or benzo(a)pyrene

Biomass-based adsorbent	Dosage (g/L)	Contact time	Removal efficiency (%)	Adsorption capacity (mg g <sup>-1</sup> )	Reference
Magnetically modified rice husk biochar	0.2	1 h	–	97.6 (PHE)	Guo et al. (2018)
Wheat straw biochar	0.6	4 h	92.2 (PHE)	–	Ding et al. (2022)
Persulfate activated by corn straw biochar	1.6	30 min	93.2 (BaP)	–	Guo et al. (2020)
Activated carbon from rice husk	0.01	1 h	98–99 (PHE)	–	Hidayat et al. (2019)
Activated carbon from banana peel	0.02	80 min	–	217.39 (PHE)	Gupta and Gupta (2016)
Activated carbon from coconut shell	0.1	1 h	99.91 (PHE)	20.22 (PHE)	Zhang et al. (2012)
Sunflower husk biochar	0.5 ng mL <sup>-1</sup>	1 h	77–81 (BaP)	–	Minkina et al. (2022)
Fe-impregnated biochar coupled with ammonium persulfate	0.01	96 h	97.2 (BaP)	–	Li et al. (2022)
Green oxide nanoparticles synthesized with pomegranate peel	0.09	150 min	99 (BaP)	–	Hassan et al. (2018)
Anthracite-based and coconut shell-based activated carbon	1.25	30 days	88 (BaP)	–	Amstaetter et al. (2012)
Activated biochar derived from palm kernel shell and palm mesocarp fiber	0.4	48 h	84–100 (PHE), 68–87 (BaP)	19.38–21.98 (PHE), 1.24–13.26 (BaP)	This study

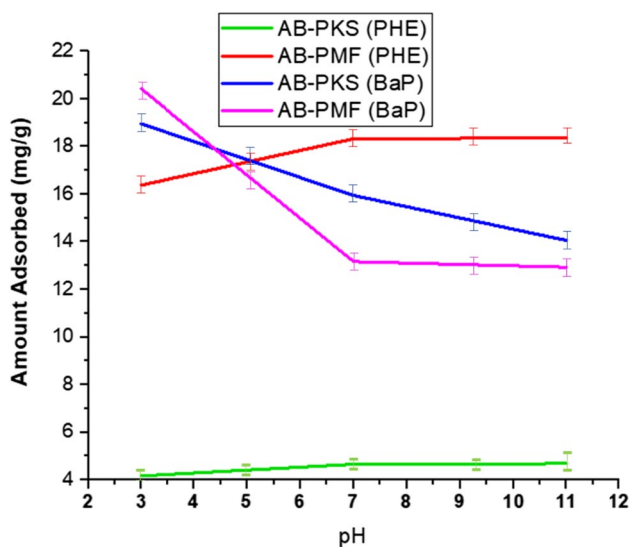


**Fig. 8** Effect of pH on phenanthrene and benzo(a)pyrene adsorption onto the various biomass-derived adsorbents (experimental conditions: concentration = 20 mg/L, dosage = 20 mg per 20 mL,  $T = 25 \pm 1$  °C, agitation rate = 150 rpm, contact time = 48 h). Error bars  $\pm$  relative standard deviation (RSD),  $n = 3$

BaP onto AB-PKS and AB-PMF. Figure 8 showed a slight increase in the adsorption for the lower molecular weight PAH (PHE) for both biomass-based adsorbents. The effect

of pH was more prominent in the heavier PAH (BaP) for both adsorbents. Furthermore, adsorption is favored at acidic pH for PHE, and deprotonation of the surface of the adsorbent at basic pH may have slightly facilitated electrostatic attraction between the PHE and the activated biochars.

The study's findings showed that the optimum pH conditions for removing PHE are < 7 and above pH 7 for BaP, respectively. At basic pH, a weak electrostatic repulsion between the negatively charged surface of the adsorbent and the electron-rich  $\pi$  systems of BaP cannot be ruled out, which would reduce the adsorption performance. The neutrality of the multiple-ringed structure of BaP could be altered by basic  $\text{OH}^-$  ions, creating negative charges around the BaP molecules and leading to electrostatic repulsion between the negatively charged surface of the material and BaP molecules under basic conditions. Nonetheless, the impact of pH on low molecular weight PAHs' overall adsorption efficiency (i.e., PHE) by biomass-based adsorbents is negligible, similar to previous studies (Adeola and Forbes 2019). The optimum dosage was established by varying the amount of AB-PKS and AB-PMS between 0.1 and 0.5 g. As shown in Fig. 9, PHE and BaP removal increased considerably with increasing amounts of sorbents, reaching between 81 and 100% for PHE and 68% and 87% for BaP, an adsorbent amount of 0.4 g/L. It was further noted that

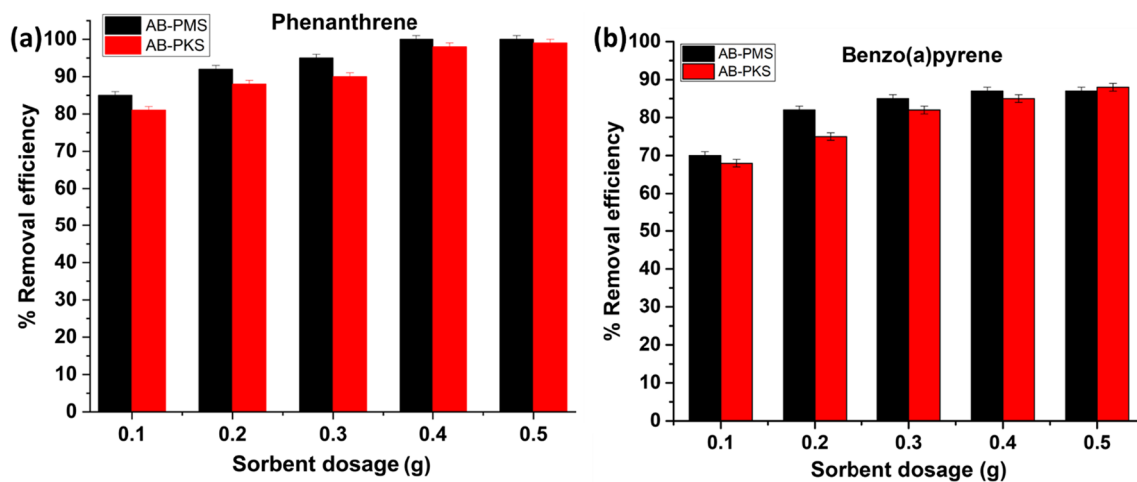


**Fig. 9** Effect of sorbent dosage on the adsorption of the selected PAHs. Error bars  $\pm$  relative standard deviation (RSD),  $n=3$

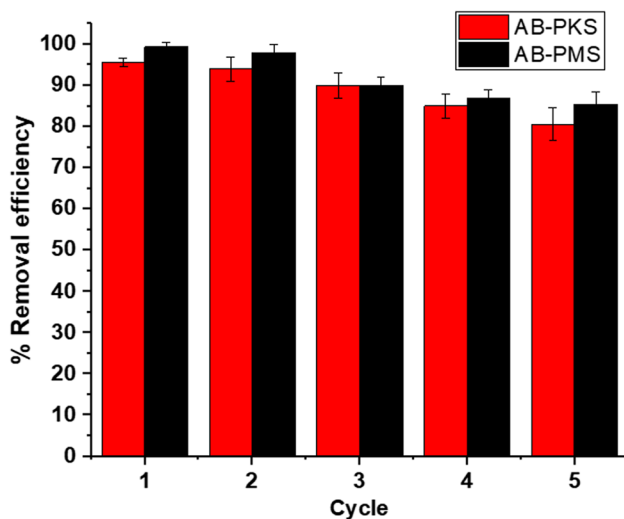


**Fig. 10** Reusability test of AB-PKS than AB-PMS for PHE adsorption (experimental conditions: 25 °C; sorbent dosage: 0.4 g; PHE concentration: 500 mg/L, acetone/water volume: 10 mL (1:1), error bars  $\pm$  relative standard deviation (RSD),  $n=3$ )

there were no significant improvements in removal performance to warrant further increment in adsorbent dosage.

### Regeneration and reusability tests

AB-PKS and AB-PMS were regenerated via a facile approach of mild rinsing with DI water and acetone. The sorbents were filtered and washed using vacuum filtration and reused in five successive adsorption cycles of PHE as a representative PAH. The sorption efficiency of AB-PMS was in the range of 99.4–85.5% and AB-PKS was between 95.7 and 80.6% over the five cycles of adsorption–regeneration as shown in Fig. 10. Irreversible pore deformation and changes

in the thermodynamic state and morphology of the material due to desorption/regeneration cycles, as well as sorbate or solvent-induced alteration of the sorbent, are several factors that may be responsible for the decline in PHE removal and stability concerns over several cycles. However, the regeneration and reusability test showed that AB-PMS can be adopted for the treatment of PAH-contaminated water for at least five cycles due to relatively better stability. Sorbent recovery was more complex for AB-PKS sorbent due to its dispersibility; hence, loss of adsorbent between cycles was higher for AB-PKS than AB-PMS.

### Conclusion

The results of this study are highly significant for potential industrial and environmental uses of adsorbents made from oil palm waste for the removal of aromatic chemicals from an aqueous medium in the context of green and sustainable chemistry. The  $q_{max}$  of the adsorbents for PHE and BaP obtained from Langmuir isotherms were 19.38–21.98 mg g<sup>-1</sup> and 1.24–13.26 mg g<sup>-1</sup>, respectively, which was among the highest values for PHE and BaP reported in the study. This study shows that the removal efficiency of PAHs from the simulated contaminated aqueous medium is 84–100% for PHE and 68–87% for BaP. It is recommended that the optimum pH conditions for removing PHE and BaP are  $<7$  and  $>7$  respectively, and an optimum sorbent dosage of 0.4 g/L for 48 h will be best suited for these biomass-derived sorbents. The sorption efficiency of AB-PMS was in the range of 99.4–85.5% and AB-PKS was between 95.7–80.6% over the five cycles of PHE adsorption and sorbent regeneration. This reveals that the removal of PAHs from contaminated water can be effectively carried out using these carbonaceous materials (AB-PKS and

AB-PMF) and that the material can be utilized in water treatment plants as a polishing tool.

**Author contributions** GN Sambo conceptualized the research, performed laboratory experiments, analyzed the data, and prepared the manuscript draft. AO Adeola conceptualized the research, analyzed the data, validated the data, and revised the manuscript. SA Muhammad supervised the study, provided funding and resources, and edited the manuscript.

**Funding** This work was supported by the Ministry of Higher Education, Malaysia under the Fundamental Research Grant Scheme (FRGS) with the grant number: FRGS/1/2022/WAB02/USM/02/2.

**Data availability** Most of the datasets used in this study have been included in the article and additional information can be accessed through the corresponding author.

## Declarations

**Conflict of interest** The authors declare that there are no conflicts of interest.

**Ethical approval** This article does not contain any studies involving human or animal subjects.

**Open Access** This article is licensed under a Creative Commons Attribution 4.0 International License, which permits use, sharing, adaptation, distribution and reproduction in any medium or format, as long as you give appropriate credit to the original author(s) and the source, provide a link to the Creative Commons licence, and indicate if changes were made. The images or other third party material in this article are included in the article's Creative Commons licence, unless indicated otherwise in a credit line to the material. If material is not included in the article's Creative Commons licence and your intended use is not permitted by statutory regulation or exceeds the permitted use, you will need to obtain permission directly from the copyright holder. To view a copy of this licence, visit <http://creativecommons.org/licenses/by/4.0/>.

## References

- Adeola AO, Forbes PBC (2019) Optimization of the sorption of selected polycyclic aromatic hydrocarbons by regenerable graphene wool. *Water Sci Technol* 80:1931–1943
- Adeola AO, Forbes PBC (2021) Advances in water treatment technologies for removal of polycyclic aromatic hydrocarbons: existing concepts, emerging trends, and prospects. *Water Environ Res* 93:343–359
- Akpmie KG, Adegoke KA, Oyedotun KO, Ighalo JO, Amaku JF, Olisah C, Adeola AO, Iwuozor KO, Conradie J (2022) Removal of bromophenol blue dye from water onto biomass, activated carbon, biochar, polymer, nanoparticle, and composite adsorbents. *Biomass Convers Biorefinery*. <https://doi.org/10.1007/s13399-022-03592-w>
- Amstaetter K, Eek E, Cornelissen G (2012) Sorption of PAHs and PCBs to activated carbon: coal versus biomass-based quality. *Chemosphere* 87:573–578
- Boretti A, Rosa L (2019) Reassessing the projections of the world water development report. *NPJ Clean Water* 2:1–6
- Bowker M (2012) Heterogeneous catalysis: fundamentals and applications. *Catal Lett* 142(11):1411–1411
- Claoston N, Samsuri AW, Ahmad Husni MH, Mohd Amran MS (2014) Effects of pyrolysis temperature on the physicochemical properties of empty fruit bunch and rice husk biochars. *Waste Manage Res* 32:331–339
- Dehghani S, Fararouei M, Rafiee A et al (2022) Prenatal exposure to polycyclic aromatic hydrocarbons and effects on neonatal anthropometric indices and thyroid-stimulating hormone in a Middle Eastern population. *Chemosphere* 286:131605
- Ding C, Gan Y, Luo J, Cui Y (2022) Wheat straw biochar and its performance in treatment of phenanthrene containing water and microbial remediation of phenanthrene contaminated soil. *Front Environ Sci* 10:2148
- Elwakeel KZ, Elgarahy AM, Mohammad SH (2017) Use of beach bivalve shells located at port said coast (Egypt) as a green approach for methylene blue removal. *J Environ Chem Eng* 5:578–587
- Feng D, Guo D, Zhang Y, Sun S, Zhao Y, Shang Q, Sun H, Wu J, Tan H (2021) Functionalized construction of biochar with hierarchical pore structures and surface O/N-containing groups for phenol adsorption. *Chem Eng J* 410:127707
- Guo W, Wang S, Wang Y, Lu S, Gao Y (2018) Sorptive removal of phenanthrene from aqueous solutions using magnetic and non-magnetic rice husk-derived biochars. *R Soc Open Sci* 5:172382
- Guo J, Wen X, Yang J, Fan T (2020) Removal of benzo (a) pyrene in polluted aqueous solution and soil using persulfate activated by corn straw biochar. *J Environ Manage* 272:111058
- Gupta H, Gupta B (2016) Adsorption of polycyclic aromatic hydrocarbons on banana peel activated carbon. *Desalin Water Treat* 57:9498–9509
- Hassan SSM, Abdel-Shafy HI, Mansour MSM (2018) Removal of pyrene and benzo (a) pyrene micropollutant from water via adsorption by green synthesized iron oxide nanoparticles. *Adv Nat Sci: Nanosci Nanotechnol* 9:15006
- Hidayat D, Supriyanto R, Permana DF (2019) Adsorption of polycyclic aromatic hydrocarbons using low-cost activated carbon derived from rice husk. In: *Journal of Physics: Conference Series*. IOP Publishing, p 12005
- Hoang AT, Nižetić S, Cheng CK, Luque R, Thomas S, Banh TL, Nguyen XP (2022) Heavy metal removal by biomass-derived carbon nanotubes as a greener environmental remediation: a comprehensive review. *Chemosphere* 287:131959
- Ibrahim A, Abdullah MF, Sam ST (2018) Hydrolysis empty fruit bunch (EFB) using green solvent. *IOP Conf Ser: Mater Sci Eng* 429:12059
- Ibrahim I, Tsubota T, Hassan MA, Andou Y (2021) Surface functionalization of biochar from oil palm empty fruit bunch through hydrothermal process. *Processes* 9:149
- Idris J, Shirai Y, Anduo Y et al (2015) Improved yield and higher heating value of biochar from oil palm biomass at low retention time under self-sustained carbonization. *J Clean Prod* 104:475–479
- Jesus F, Pereira JL, Campos I et al (2022) A review on polycyclic aromatic hydrocarbons distribution in freshwater ecosystems and their toxicity to benthic fauna. *Sci Total Environ*. <https://doi.org/10.1016/j.scitotenv.2022.153282>
- Jouiad M, Al-Nofeli N, Khalifa N et al (2015) Characteristics of slow pyrolysis biochars produced from rhodes grass and fronds of edible date palm. *J Anal Appl Pyrol* 111:183–190
- Kubheka G, Adeola AO, Forbes PBC (2022) Hexadecylamine functionalised graphene quantum dots as suitable nano-adsorbents for phenanthrene removal from aqueous solution. *RSC Adv* 12:23922–23936
- Li X, Yu Z, Chen Q et al (2022) Kill three birds with one stone: Iron-doped graphitic biochar from biogas residues for ammonium persulfate activation to simultaneously degrade benzo [a] pyrene and improve lettuce growth. *Chem Eng J* 430:132844



- Minkina T, Vasilyeva G, Popileshko Y et al (2022) Sorption of benzo [a] pyrene by Chernozem and carbonaceous sorbents: comparison of kinetics and interaction mechanisms. *Environ Geochem Health* 44:133–148
- Nascimento P, Marim R, Carvalho G, Mali S (2016) Nanocellulose produced from rice hulls and its effect on the properties of biodegradable starch films. *Mater Res* 19:167–174
- Natsir M, Ansharullah A, Maulidiyah M, Herikiswanto H, Sari A, Salim LOA, Nurdin M (2021) Decomposition of lignin compounds from oil palm empty fruit bunch using ilmenite. *J Phys: Conf Ser* 1899:12044
- Nnaji CC, Agim AE, Mama CN et al (2021) Equilibrium and thermodynamic investigation of biosorption of nickel from water by activated carbon made from palm kernel chaff. *Sci Rep* 11:1–20
- Nurhafizah MD, Sabar I, Suriani AB, Mohamed A (2020) Graphene oxide/low ammonia NRL nanocomposite-based electrode in various electrolyte concentrations: electrical properties and capacitive behavior for supercapacitor. *J Rubber Res* 23:387–393
- Pathak U, Jhunjhunwala A, Roy A et al (2020) Efficacy of spent tea waste as chemically impregnated adsorbent involving orthophosphoric and sulphuric acid for abatement of aqueous phenol—isortherm, kinetics and artificial neural network modelling. *Environ Sci Pollut Res* 27:20629–20647. <https://doi.org/10.1007/s11356-019-06014-z>
- Pavlenko V, Żółtowska S, Haruna AB, Zahid M, Mansurov Z, Supiyeva Z, Galal A, Ozoemena KI, Abbas Q, Jesionowski T (2022) A comprehensive review of template-assisted porous carbons: modern preparation methods and advanced applications. *Mater Sci Eng: R: Rep* 149:100682
- Pltonykova H, Koeppl S, Bernardini F, et al (2020) The united nations world water development report 2020: Water and climate change.
- Priyadarshini I, Alkhayyat A, Obaid AJ, Sharma R (2022) Water pollution reduction for sustainable urban development using machine learning techniques. *Cities* 130:103970
- Roy S, Das P, Mukhopadhyay A (2021) Biochar from waste *Sterculia foetida* and its application as adsorbent for the treatment of PAH compounds: batch and optimization. *Fuel* 306:121623. <https://doi.org/10.1016/j.fuel.2021.121623>
- Saleh S, Abdul Samad NAF (2022) Modeling of volatile composition during heating and isothermal stages of the torrefaction process. *Chem Eng Technol* 45:1467–1473
- Saleh M, Bilici Z, Ozay Y, Yabalak E, Yalvac M, Dizge N (2021) Green synthesis of *Quercus coccifera* hydrochar in subcritical water medium and evaluation of its adsorption performance for BR18 dye. *Water Sci Technol* 83(3):701–714. <https://doi.org/10.2166/wst.2020.607>
- Sambo G, Muhammad SA, Pyar HA, Binhwel F (2022) Treatment of water contaminated with polycyclic aromatic hydrocarbons (PAHs): a review of various techniques, constraints, and field procedures. *Chimica Et Nat Acta* 10:33–52
- Tan IAW, Abdullah MO, Lim LLP, Yeo THC (2017) Surface modification and characterization of coconut shell-based activated carbon subjected to acidic and alkaline treatments. *J Appl Sci Process Eng* 4:186–194
- Wan Isahak WNR, Hamzah N, Nordin NAM, Mohamed HMW, Yarmo MA (2013) Dehydration studies of biomass resources for activated carbon production using BET and XRD techniques. *Adv Mater Res* 620:491–495
- Wang J, Chen Z, Chen B (2014) Adsorption of polycyclic aromatic hydrocarbons by graphene and graphene oxide nanosheets. *Environ Sci Technol* 48:4817–4825
- Zhang C, Zhang X, Huang Z, Huang D, Cheng Q (2012) Adsorption and de-sorption of polycyclic aromatic hydrocarbons on activated carbon. *J Environ Anal Toxicol* 2:1–6
- Zhang YL, Liu YJ, Dai CM, Zhou XF, Liu SG (2014) Adsorption of clofibric acid from aqueous solution by graphene oxide and the effect of environmental factors. *Water Air Soil Pollut* 225:1–10
- Zhou X, Shi L, Moghaddam TB et al (2022) Adsorption mechanism of polycyclic aromatic hydrocarbons using wood waste-derived biochar. *J Hazard Mater* 425:128003
- Zou SJ, Chen YF, Zhang Y et al (2021) A hybrid sorbent of  $\alpha$ -iron oxide/reduced graphene oxide: studies for adsorptive removal of tetracycline antibiotics. *J Alloy Compd* 863:158475

**Publisher's Note** Springer Nature remains neutral with regard to jurisdictional claims in published maps and institutional affiliations.